

## Supporting Information for

# **The added value of new ground-based observations in improving China's methane emission quantification**

5

Huiru Zhong<sup>1</sup>, Lu Shen<sup>1</sup>, Fengwei Wan<sup>1</sup>, Meng Qu<sup>1</sup>, Kai Qin<sup>2</sup>

<sup>1</sup>Department of Atmospheric and Oceanic Sciences, School of Physics, Peking University, Beijing 100871, China

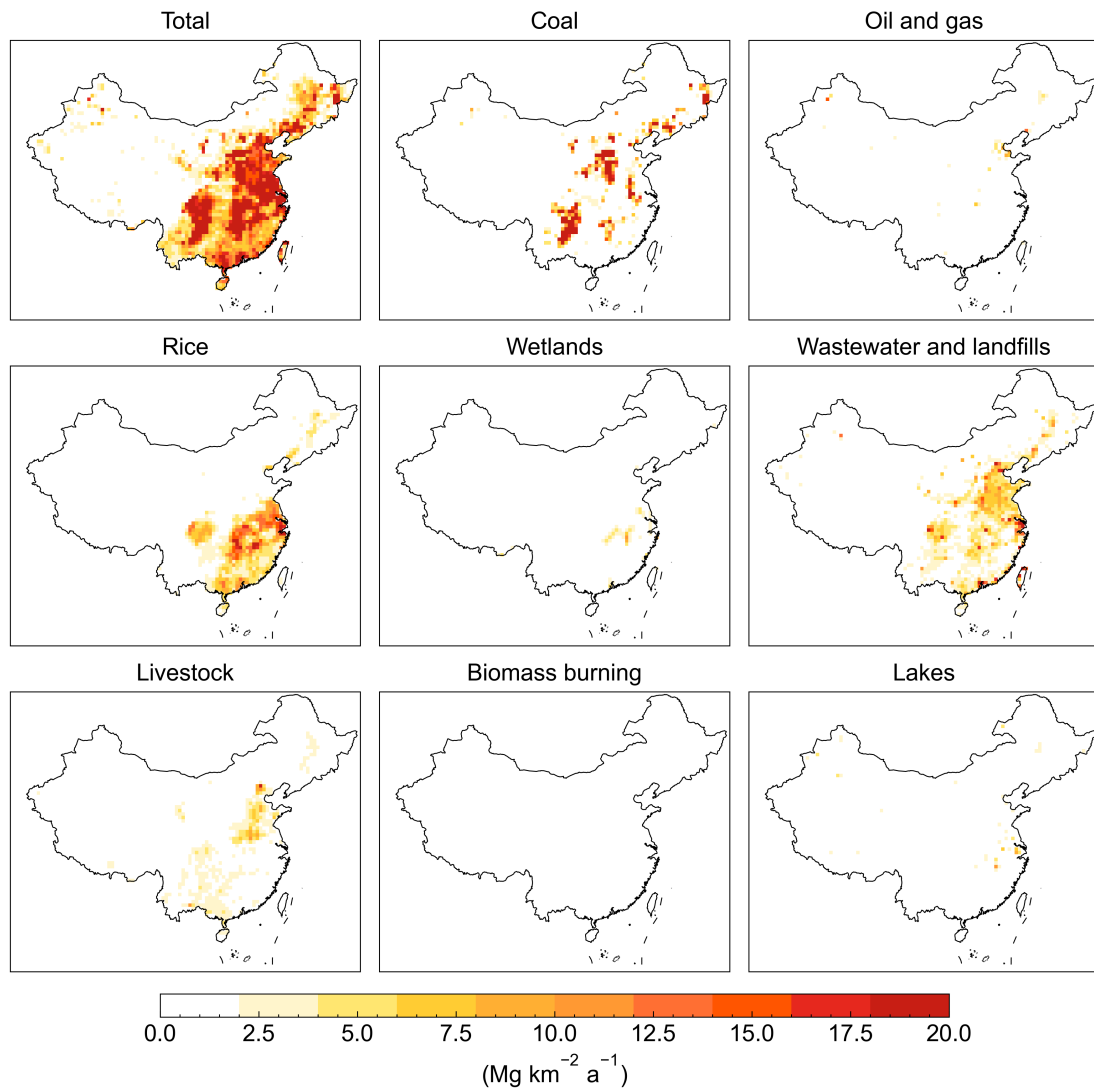
<sup>2</sup>Jiangsu Key Laboratory of Coal-Based Greenhouse Gas Control and Utilization, School of Environment and Spatial Informatics, China University of Mining and Technology, Xuzhou, China

10 *Correspondence to:* Lu Shen ([lshen@pku.edu.cn](mailto:lshen@pku.edu.cn))

### **Contents of this file**

Figures S1-S5

### Spatial distribution of prior methane emissions by sector



15

**Figure S1.** Spatial distribution of prior methane emissions by sector in China. Emissions for energy sectors (coal, oil and gas) are from Global Fuel Exploitation Inventory version 2.0 (GFEIv2) (Scarpelli et al., 2022). Other anthropogenic methane emissions are from Emission Database for Global Atmospheric Research (EDGARv6) inventory (Ferrario et al., 2021) and wetland methane emissions are from the mean of 18 members of the WetCHARTs v1.3.1 inventory ensemble (Ma et al., 2021). Termite methane emissions are from Fung et al., (Fung et al., 1991), and aquatic system methane emissions are from Johnson et al., (Johnson et al., 2022).

20

# Comparison of methane concentrations between observations and GEOS-Chem prior simulations

## (a) TCCON dataset

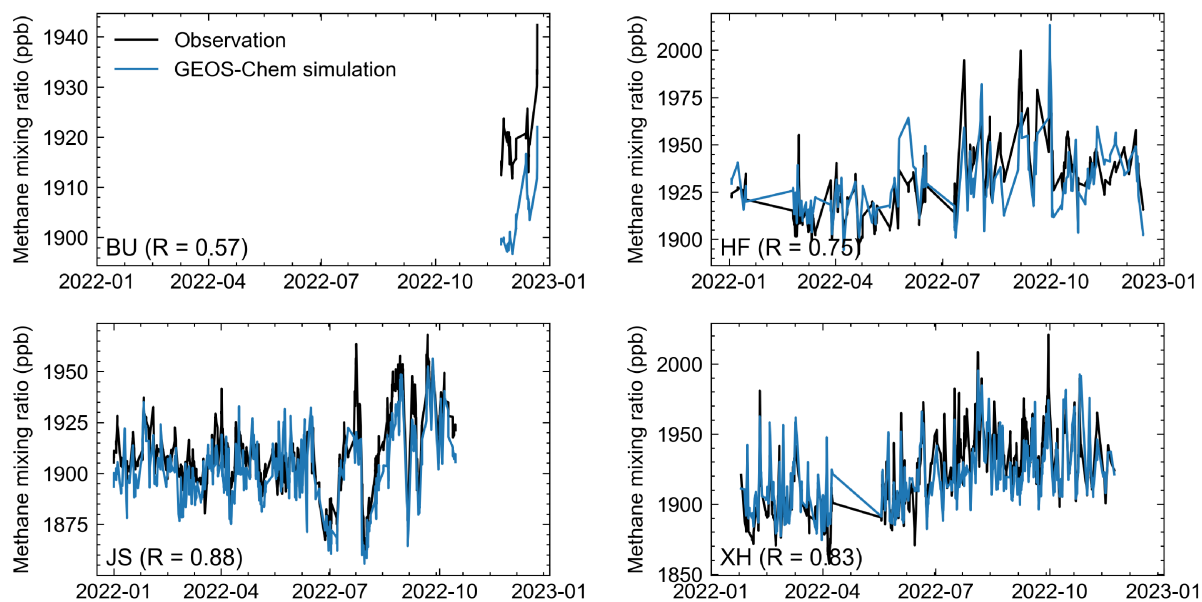


**Figure S2.** Comparison of methane concentrations between observations and GEOS-Chem prior simulations. Methane observations (ppb) from (a) TCCON XCH<sub>4</sub> and (b) ObsPack v7.0 surface CH<sub>4</sub> concentrations. The lower-left corner of each panel indicates the correlation coefficient between the observations and the simulations. (Continued on next page.)

25

(b) Obspack v7.0 dataset

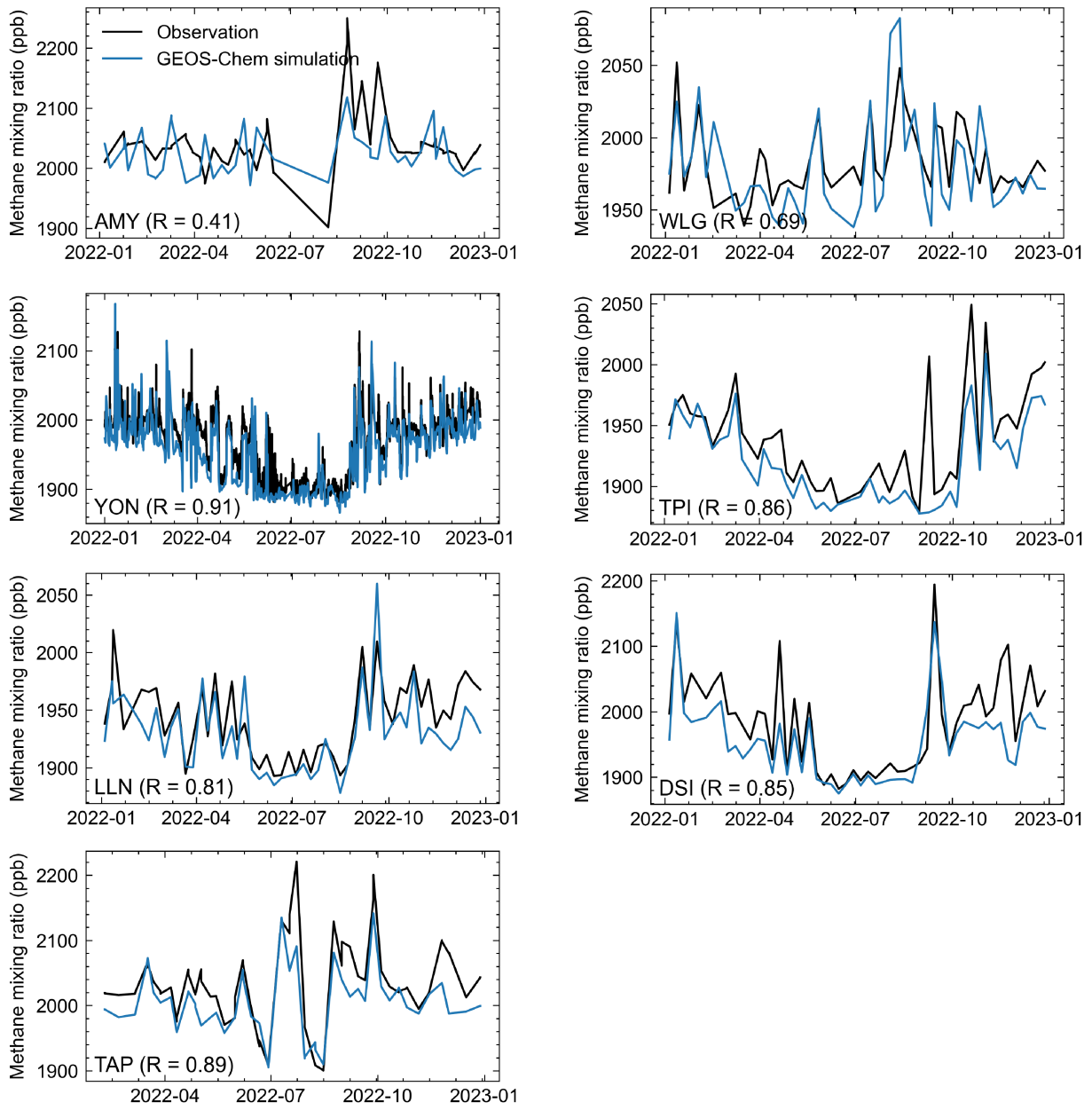
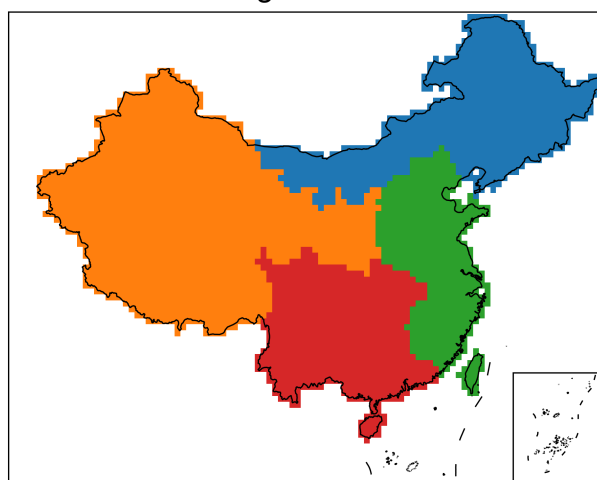


Figure S2. (continued).

Four regions of China



**Figure S3.** Regional division of China into four areas for regional DOFS analysis. Northeast (blue), Northwest (orange), Southeast (green), and Southwest (red). Inner Mongolia is divided between Northeast and Northwest regions based on its longitudinal extent.

(a) Optimized surface station networks for monthly sampling frequency

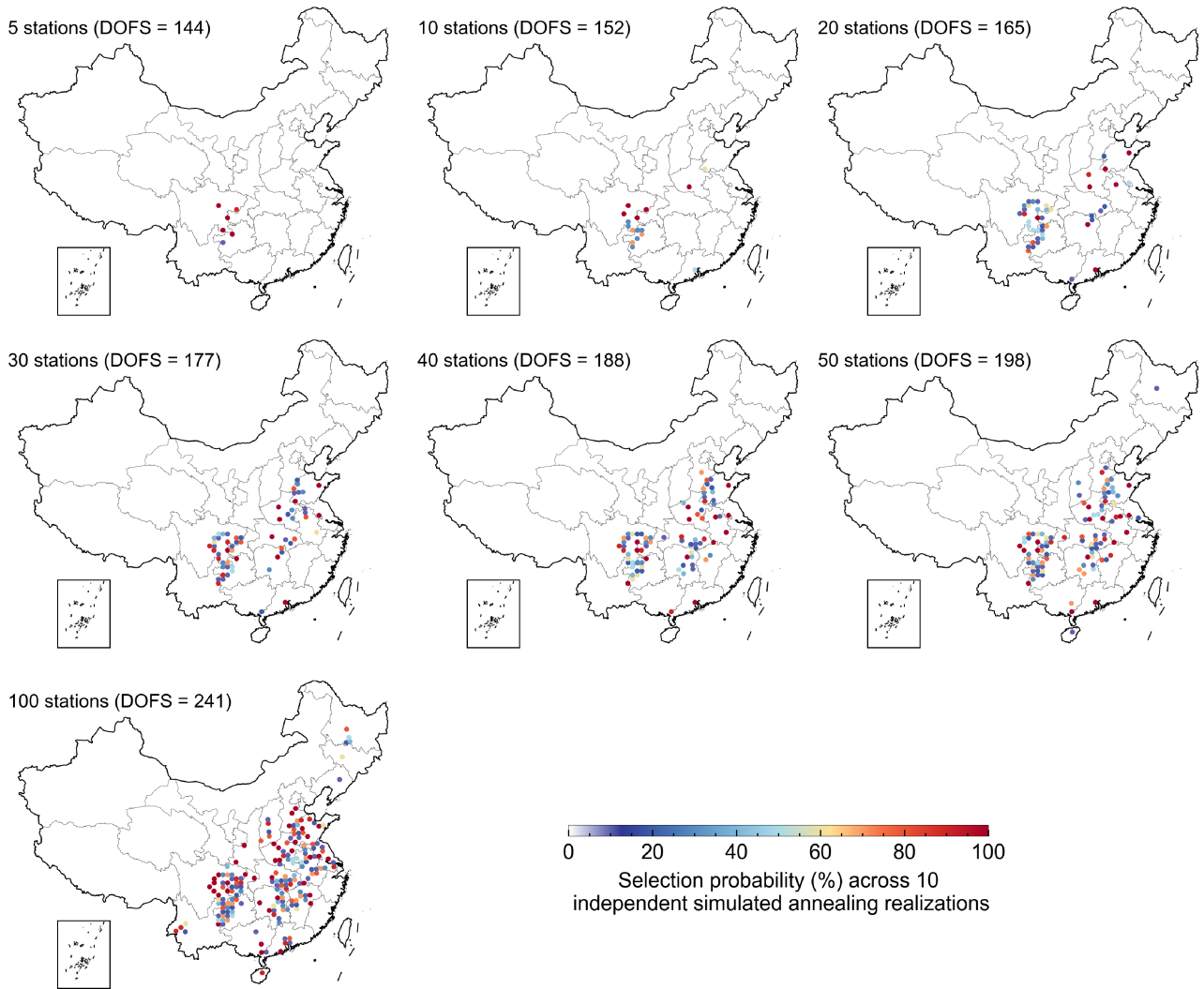


**Figure S4.** Optimized surface station networks for monthly and daily sampling frequencies. **(a)** Monthly sampling frequency. **(b)** Daily sampling frequency. The panels show the selection probability (%) of each grid cell for a new site across 10 independent simulated annealing realizations, spanning network sizes of 5 to 100 new stations. The corresponding increase in the degrees of freedom for signal (DOFS) is displayed within each panel. (Continued on next page.)

40

(b) Optimized surface station networks for daily sampling frequency

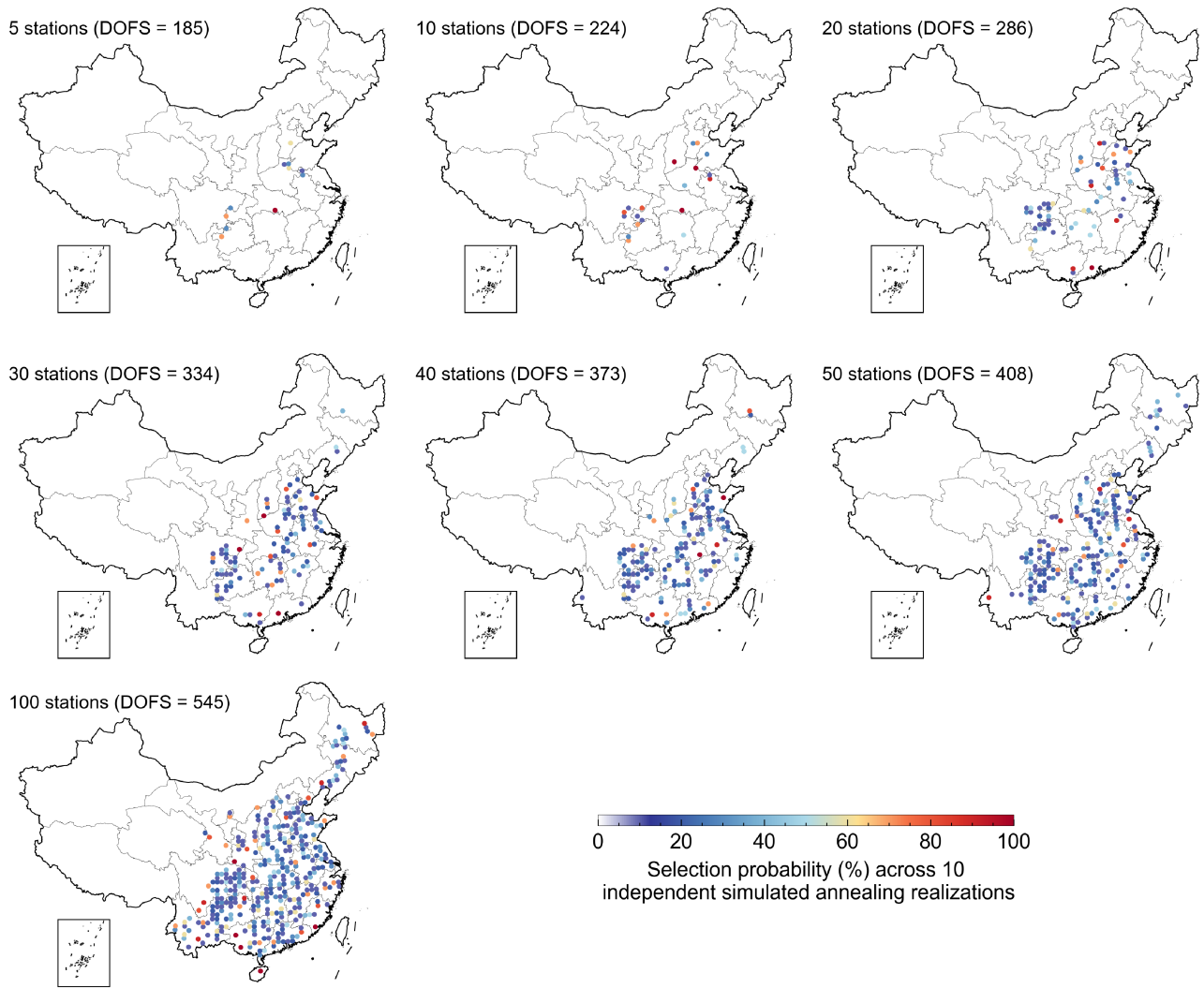
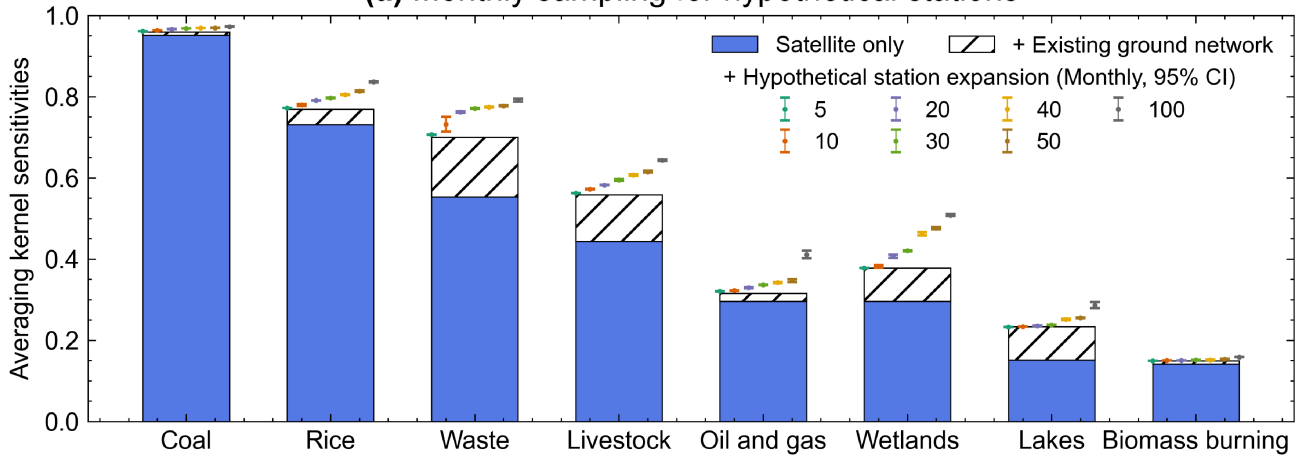


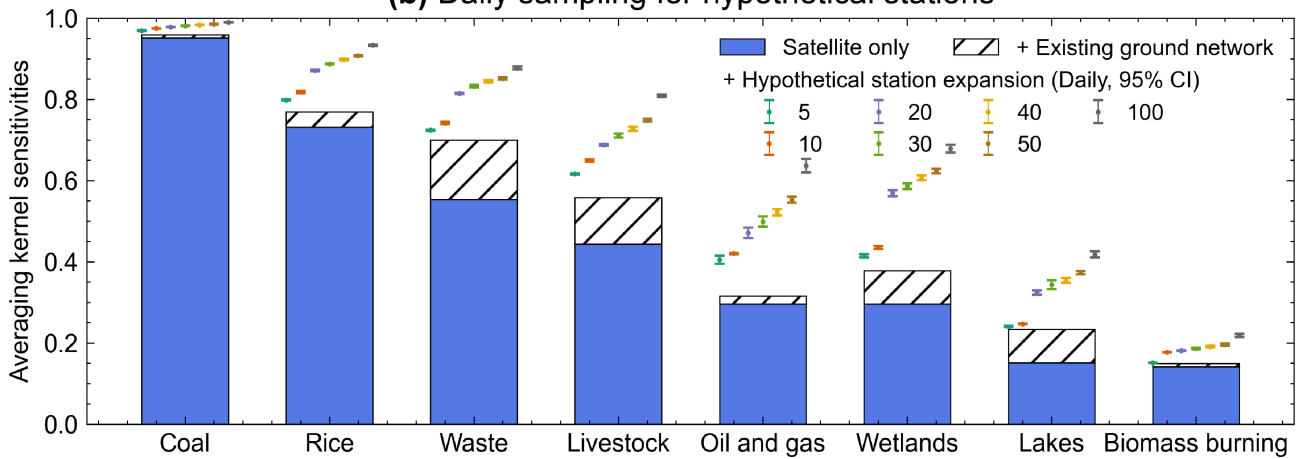
Figure S4. (continued).

## Observational constraints on sectoral methane emissions in China

**(a) Monthly sampling for hypothetical stations**



**(b) Daily sampling for hypothetical stations**



45

**Figure S5.** Observational constraint on sectoral methane emissions in China under different observational networks. Panel (a) shows results for hypothetical stations with monthly sampling frequency, and panel (b) shows results for hypothetical stations with daily sampling frequency. The blue bars represent AK sensitivities derived from TROPOMI observations alone, while the hatched bars represent the increase in AK sensitivities achieved by incorporating the existing ground-based measurements. Colored error bars show the mean AK sensitivities and 95% confidence interval (95% CI) from 10 simulated annealing experiments.

50

## References

- 55 Ferrario, F. M., Crippa, M., Guizzardi, D., Muntean, M., Schaaf, E., Vullo, E. L., Solazzo, E., Olivier, J., and Vignati, E.: EDGAR v6.0 Greenhouse Gas Emissions, 2021.
- Fung, I., John, J., Lerner, J., Matthews, E., Prather, M., Steele, L. P., and Fraser, P. J.: Three-dimensional model synthesis of the global methane cycle, *J. Geophys. Res.*, 96, 13033–13065, <https://doi.org/10.1029/91JD01247>, 1991.
- Johnson, M. S., Matthews, E., Du, J., Genovese, V., and Bastviken, D.: Methane emission from global lakes: new spatiotemporal data and observation-driven modeling of methane dynamics indicates lower emissions, *J. Geophys. Res. Biogeosci.*, 127, e2022JG006793, <https://doi.org/10.1029/2022JG006793>, 2022.
- 60 Ma, S., Worden, J. R., Bloom, A. A., Zhang, Y., Poulter, B., Cusworth, D. H., Yin, Y., Pandey, S., Maasakkers, J. D., Lu, X., Shen, L., Sheng, J., Frankenberg, C., Miller, C. E., and Jacob, D. J.: Satellite constraints on the latitudinal distribution and temperature sensitivity of wetland methane emissions, *AGU Adv.*, 2, e2021AV000408, <https://doi.org/10.1029/2021AV000408>, 2021.
- 65 Scarpelli, T. R., Jacob, D. J., Grossman, S., Lu, X., Qu, Z., Sulprizio, M. P., Zhang, Y., Reuland, F., Gordon, D., and Worden, J. R.: Updated global fuel exploitation inventory (GFEI) for methane emissions from the oil, gas, and coal sectors: evaluation with inversions of atmospheric methane observations, *Atmos. Chem. Phys.*, 22, 3235–3249, <https://doi.org/10.5194/acp-22-3235-2022>, 2022.